Journal of Molecular Liquids 395 (2024) 123881

Contents lists available at ScienceDirect

Journal of Molecular Liquids

journal homepage: www.elsevier.com/locate/molliq

Hydration water and ionic aggregation in aqueous solutions of imidazolium-based protic ionic liquids

F. Matroodi [a,b,*], C. Bottari [b], B. Rossi [b], A. Mannu [c], M. Paolantoni [d,*], A. Mele [c]

[a] Department of Physics, Shahid Chamran University of Ahvaz, Ahvaz, Iran
[b] Elettra Sincrotrone Trieste, S.S. 114 km 163.5, Basovizza, 34149 Trieste, Italy
[c] Department of Chemistry, Materials and Chemical Engineering "G. Natta", Politecnico di Milano, Piazza L. da Vinci 32, 20133 Milano, Italy
[d] Department of Chemistry, Biology and Biotechnology, University of Perugia, Via Elce di Sotto 8, 06123 Perugia, Italy

ARTICLE INFO

Keywords:
Imidazolium
Hydration water
Protic ionic liquids
UV Resonance Raman
Solute-correlated Raman spectra

ABSTRACT

Water molecules, present as additive or as contaminant of Protic Ionic Liquids (PILs), can compete for the hydrogen bond sites leading to important modifications of the local order of these liquids and to the modulation of their physical–chemical properties. In this work, aqueous solutions of a set of N-methylimidazolium-based PILs [MIM][X] (X = NO_3^-, TfO^-, HSO_4^-, and Cl^-) were investigated by deep UV Resonance Raman (UVRR) spectroscopy in the water-rich domain where ionic aggregates and bulk-like water coexist. A differential method was used to analyze the OH stretching profile to extract the so-called solute-correlated (SC) spectrum, which is particular informative of the hydration features of the PILs. Moreover, specific bands of the cation, sensitive to the hydrogen bonding, were comparatively investigated. The progressive evolution from solvent-separated ion pairs (SIP) and/or solvent-shared ion pairs (SSIP) to contact ion pairs (CIP) and/or larger ionic aggregates can be monitored as a function of the hydration level, in the water-rich domain. Our approach showed that, in the high-diluted regime, the hydration environment around the [MIM] cation does not depend on the type of anion. Moreover, [MIM][NO_3] and [MIM][TfO] showed cation-water (ionic) H-bonds at the NH site stronger than the cation–anion (double-ionic) ones. The analysis of SC Raman spectra points out the formation of cation–anion H-bonds (through the CH ring groups), stronger than cation-water ones, upon PILs concentration increase, especially evident in the case of [MIM][Cl]. The H-bond strength between the anion and hydration water is found to decrease following the order: [Cl] ~ [HSO_4] > [NO_3] > [TfO]. Chloride ions tend to perturb a larger number of water molecules than the other anions. The number of perturbed water molecules decreases at increasing PIL concentration, showing a larger dependence for [MIM][Cl], consistently with its larger propensity to form ionic aggregates. The unique response of [MIM][Cl] to hydration found by analyzing SC-UVRR data is related to the synergy of different factors such as the anion reduced size (higher charge density), spherical symmetry, and high H-bond basicity.

1. Introduction

Protic ionic liquids (PILs) are an interesting subset of the large family of room temperature ionic liquids – RTILs or simply ILs [1] – characterized by the presence of acidic protons within the molecular frame of the cation [2,3]. PILs' popularity is constantly growing as they merge the general properties of ILs with the easy preparation procedure, which very often consists of a single acid-base reaction between suitable components. The presence of activated H atoms on the cation, such as N—H in imidazolium based PILs, provides PILs with a stronger hydrogen bond (H-bond) donor capability compared to "normal", aprotic ionic liquids, often referred to as AILs (e.g. N,N-dialkylimidazolium based ILs). In fact, it has been demonstrated that H-bonds might significantly contribute to total cation–anion interactions in both AILs and PILs [4–6] and that the relative contribution between H-bonding and Coulombic interactions can be enhanced going from AILs to PILs [5]. To note that increasing the H-bonding contribution in ILs can even lower their viscosity and melting points [6]. Fumino et al. [7] studied three alkylammonium nitrates by far FTIR, showing that PILs can form a 3-dimensional H-bond network similar to water, although the structural features of the ammonium cation and the planar geometry of the nitrate prevent a tetrahedral arrangement.

* Corresponding authors.
E-mail addresses: matroodi@gmail.com (F. Matroodi), marco.paolantoni@unipg.it (M. Paolantoni).

https://doi.org/10.1016/j.molliq.2023.123881
Received 15 May 2023; Received in revised form 17 December 2023; Accepted 21 December 2023
Available online 27 December 2023

Thus, PILs are potentially expected to form extended H-bonding networks by using both the proton-donor and proton-acceptor sites present in their chemical structure [2,3]. One important consequence of this fact is that the water molecules, present as additive or as contaminant, can compete for the H-bond sites leading to important modifications of the local order of the PIL and modulation of their physical–chemical properties [8]. In general, the contamination with traces of water was originally considered an important drawback from the application viewpoint of both AILs and PILs. However, the recent literature pointed out the modern trend of exploiting the presence of water to enhance or to modulate the properties of materials, as for the paradigmatic – but not exhausting – cases of the water-in-salt systems for state-of-the-art energy devices [9], aqueous ILs solutions for oil recovery [10], ILs as co-solvents to decrease water surface tension [11] or ILs as additive to improve the performance of aqueous Zn-ion batteries [12]. Experimental and theoretical calculations demonstrate that water-anion interactions would play a fundamental role in determining the solubility of water in ILs, even if the contribution of cation-water interactions is expected to be relevant also in AILs [4].

The beneficial effect of the addition of small or large quantity of water to PILs for biological [13–16] and electrochemical applications [17–20] is currently well assessed. PILs were reported to exhibit a noticeably stronger interaction with water compared to AILs, mainly for the larger capability of the former to establish H-bonds [15,21]. The PILs H-bonding network can be partially disrupted by the addition of water and the strong cation–anion interactions can be replaced by cation-water and anion-water ones as the water content increases [22–26]. In this respect the progressive addition of water tends to reduce the stability of contact ion pairs (CIP), favoring the formation of solvent-shared ion pairs (SSIP) and solvent-separated ion pairs (SIP) [25,26]. In this respect, in the case of the PIL triethylammonium methylsulfonate $[Et_3NH][CH_3SO_3]$ (TEAMS), it was found that at least 80 mol % water is necessary to favor SIP over CIP [26]. Several important factors such as the steric hindrance of the PILs, their hydrophilic/hydrophobic balance [27], the nature of cation and anion, the water content, and the temperature [26,28] should be considered in describing the complex hydration process. Bailey et al. used optical heterodyne-detected optical Kerr effect (OHD-OKE) spectroscopy and FTIR to compare the behavior of one PIL $[EHIM][NTf_2]$ to its aprotic counterpart $[EMIM][NTf_2]$ at different water concentrations. They reported that the capability of the PIL in making strong H-bonds caused a dramatic change in its friction coefficient by hydration. In opposite, the aprotic analogue showed limited interactions with water for all concentrations [29].

A thorough investigation of the intermolecular interactions in ILs-water binary mixtures can be achieved by FTIR and Raman spectroscopies [30], thanks to the capability of these vibrational techniques in detecting the local changes occurring around a probing oscillator. Spectroscopy studies on the hydration effect on imidazolium-based AILs showed that the addition of water to ILs causes significant blue shifts of the signals assigned to the stretching vibrations of both C(2)—H and C(4,5)—H bonds [31,32]. This has been attributed to the progressive weakening of cation–anion interactions due to the formation of weaker cation-water ones, which lead to the ion pair dissociation at higher water content. Similar studies involving imidazolium-based PILs, where the contribution of H-boding interactions should be relatively more important, have been more rarely considered. In the present manuscript we report on the behavior of a set of imidazolium-based PILs mixed with water in the water-rich domain, investigated by UV Resonance Raman (UVRR) spectroscopy. Pre-resonance conditions in deep UV excitation enhance the Raman cross section of imidazolium ring vibrations and makes it possible to investigate the vibrational signals of PILs even in water-rich mixtures [33]. Thanks to the marked increment of the detection limit due to the resonance enhancement and to the suppression of interfering fluorescence contributions, the Raman signals arising from both PILs and water can be separately detected and analyzed. A detailed description of the first hydration shell of the selected PILs is here proposed by the analysis of the OH stretching region, according to the method introduced by Ben-Amotz et al. [34–39], providing the so-called solute-correlated spectrum (SC). This latter represents the spectral contribution arising from the layer of water molecules more strongly affected by the anions, thus giving unique structural details on the hydration process. In this study, the UVRR spectra of four PILs of general formula [MIM][X], with [MIM] = N-methylimidazolium cation and [X] = HSO_4^-, NO_3^-, TfO^- and Cl^- are collected and compared at different hydration conditions. The chosen anions show different H-bond acceptor capability, as described by their β solvatochromic parameter [40–43], size and charge delocalization. The rationale behind this work is a comparative exploration of how the increasing addition of water can modify the strength and distribution of intermolecular H-bonds in model methylimidazolium-based PILs, an IL class relatively less studied than the AIL counterpart. In particular, we aim to elucidate i) the local H-bonding properties of the cation and their changes induced by added water in the water-rich domain, when ionic aggregates and bulk-like water are expected to coexist; ii) the nature of the water-PIL interactions, with particular emphasis on the water hydrating the anion; iii) the modulation effect exerted by different anions on the above features.

2. Experimental methods

2.1. Sample preparation

For the sake of clarity, the following notation will be used throughout the paper. The species in squared brackets are ions whose charge is understood. The explicit charge symbol is reported only if the chemical formula is without brackets. 1-methylimidazolium hydrogen sulfate [MIM][HSO_4] was purchased from Sigma Aldrich with a purity of 95 %. 1-methylimidazolium chloride [MIM][Cl], 1-methylimidazolium trifluoromethylsulfonate [MIM][TfO] and 1-methylimidazolium nitrate [MIM][NO_3] were purchased from IoLiTec with a purity of 99 %. High-purity water, deionized through a MilliQTM water system (>18 MΩ cm resistivity), was used for all the experiments. IL/H_2O solutions were prepared in a dry glove box at different PIL molar fraction defined as $x_{IL} = n_{IL}/(n_{IL} + n_{H_2O})$, where n_{IL} and n_{H_2O} represent the mole number of PIL and water, respectively. The molecular structures of ILs used in this study are reported in Table 1 together with the atom labeling used in the following.

2.2. UVRR experiments and data analysis

UVRR experiments were carried out at the BL10.2-IUVS beamline of Elettra Sincrotrone Trieste (Italy) by exploiting the multi-wavelengths UVRR setup [43,44]. The Raman spectra were collected using the excitation wavelength at 266 nm provided by a CryLas FQSS 266-Q2 diode pumped passively Q196 switched solid-state laser. All UVRR spectra were acquired in back-scattered geometry using a single pass of a Czerny–Turner spectrometer (Trivista 557, Princeton Instruments, 750 mm focal length) equipped with a holographic grating at 1800 and 3600 grooves per mm. The spectral resolution was set at 1.7 cm^{-1}/pixel. The calibration of the spectrometer was standardized using cyclohexane (spectroscopic grade, Sigma Aldrich). The power of the beam on the sample was kept sufficiently low (hundreds of μW) in order to avoid photo-damage effects and heating of the sample. Any possible photo-damage effect due to prolonged exposure of the sample to UV radiation was avoided by continuously spinning the sample cell during the measurements. The spectra collection of the dehydrated ILs in their liquid state was done at temperatures above their melting points, i.e. T = 355 K, 368 K, 325 K, and 360 K for [MIM][X], with [X] = [NO_3], [TfO], [HSO_4], and [Cl], respectively, as reported in Table 1. UVRR spectra have been treated first by polynomial baseline correction, then the spectra are smoothed by Savitzk-Golay second order, 14 points of window. The deconvolution of the spectra has been done using a sum of

Table 1
Molecular structure, atom numbering and melting temperature of the four PILs analyzed in the work. The atom numbering used for the assignment of the main vibrational peaks is reported.

Sample	Melting temperature (K)	Molecular structure cation, anion
[MIM][NO_3]	339	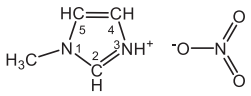
[MIM][TfO]	357	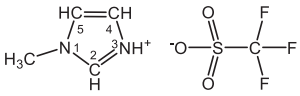
[MIM][HSO_4]	312	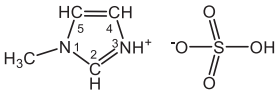
[MIM][Cl]	352	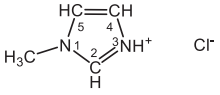

Pseudo-Voigt functions available in Origin Lab software. Solute-correlated (SC) spectra [34,35] were obtained from the OH stretching distribution by a direct spectral subtraction procedure, as the difference between the spectrum of the PILs/water mixture and a properly rescaled spectrum of neat water [39]. The rescaling factor is determined in such a way that the resulting difference distribution is non-negative and with the minimum area [38].

3. Results and discussion

The UVRR spectra of water-rich mixtures of [MIM][X] were collected as a function of IL molar fraction ($0.005 < x_{IL} < 0.4$) in the spectral range from 600 to 4000 cm^{-1}. The analysis of the spectra provides a picture of the system on the intermolecular scale and with a marked sensitivity and selectivity to specific molecular moieties assigned to the PILs and to the water molecules. The region between 1000 and 1600 cm^{-1} of the Raman spectrum provides insights on the molecular interactions that specifically involve the cations of PILs in the water-PIL mixtures. UV–VIS absorption spectra (see Supplementary Material, Fig. S1) suggest that [MIM] strongly absorbs in the UV spectral region below 250 nm. Previous works evidenced that the excitation wavelength $\lambda = 266$ nm is close enough to the resonance conditions to significantly increase the intensity of the Raman peaks associated to the cation [33]. These signals are sensitive spectroscopic markers for tracking changes of intermolecular interactions occurring around the cations upon the progressive addition of water. Before any discussion on the collected spectra in terms of the possible intermolecular interactions among the components – cations, anions and water molecules –, it is worth summarizing here some key concepts about the H-bonding in imidazolium PILs. Fig. 1 (Panel A) draws a general – although not exhaustive – scheme of the H-bond interactions between MIM^+ and a generic X^- anion. Fig. 1A is adapted from Fig. 4 of the reference paper by Hunt et al. [39]. In our case, the pristine PILs show H-bond interactions between two ionic species, commonly referred to as "double ionic" H-bonds and sketched in the Panel A as the dotted lines. Fig. 1 is a first approximation pictorial sketch here proposed as a guide for the eye, considering the following facts on H-bond in ILs: i) the [MIM] cation has two sites of primary H-bond donation, e. g. the C(2)—H and the N—H. For the sake of comparison, the aprotic imidazolium cations (such as 1-methyl-3-butylimidazolium [BMIM] present in a large set of AILs) show the C(2)—H bond as the only primary H-bond site; ii) strictly speaking, the "donor strength" of N—H is considered bigger that C—H. In imidazolium cation, however, the C(2)—H site is quite a strong donor due to the activation provided by the N atoms in position 1 and 3 of the ring. Conversely, C(4)—H and C(5)—H are ranked as weaker donor sites than C(2)—H; iii) $C(sp^3)$—H bonds do possess weak but significant H-bond donor capability and can be fully involved in multicentric interactions, as in Panel A (Front-Me and Side-Me); iv) out-of-plane H-bonds are also known, with the H-bond acceptor ion above and below the five membered ring.

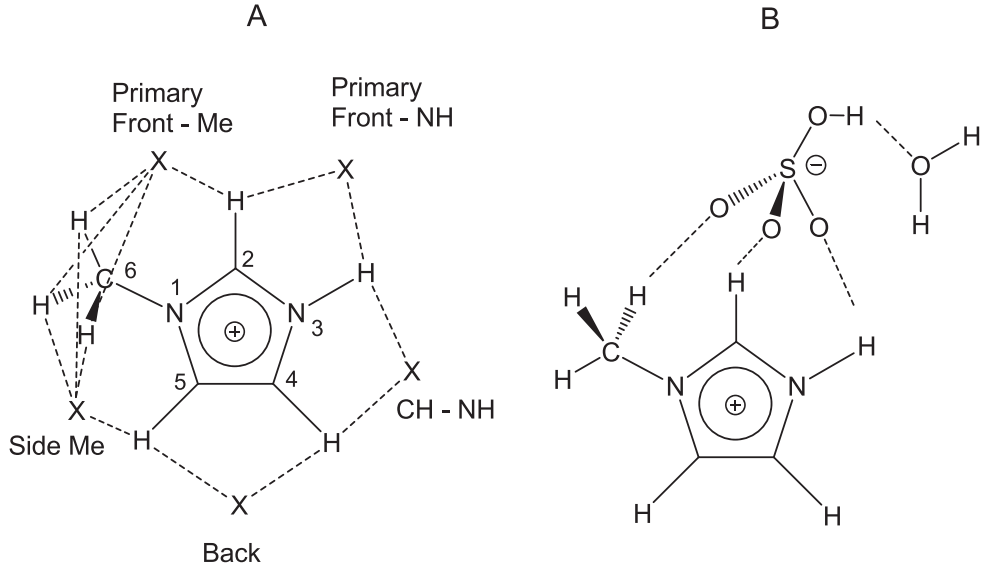

Fig. 1. Panel (A): sketch of the main types of H-bond interactions between the PIL cation and a hydrogen bond acceptor X. The nomenclature is adapted from ref. [43]. Atom numbering is as in Table 1. Panel (B): sketch of multicentric double-ionic H-bond network with participation of water.

However, no attempt has been done to sketch this class of H-bonds in Fig. 1; v) in imidazolium PILs the N—H group does not generally transfer H^+ to the H-bond acceptor via acid-base equilibrium [43]; vi) it should be kept in mind that the number of possible H-bond patterns in PIL is larger compared to AILs, for the presence of a larger number of protic groups. This fact may lead to complex supramolecular architectures, especially in the presence of anions and water molecules acting as H-bond competitors. For clarity, one sketch is shown in Fig. 1, panel B.

To investigate the role played by the anion in modulating hydration effects in the four selected PILs, we first compared the Raman spectra of the pure ILs above their melting point (i.e. in their liquid state). The resulting UVRR spectra collected using 266 nm as excitation wavelength for the four samples are shown in Fig. 2.

For each sample, the Raman spectra have been collected at the temperatures indicated in the Fig. 2, above the PILs melting point to ensure that the systems were in the liquid state. Only small changes on the positions of the bands were observed by ATR-FTIR spectroscopy at different temperatures for the neat liquids (data not shown). Some selected Raman bands (marked by dotted lines in Fig. 2) were chosen as useful descriptors of the state of the imidazolium cation, being not significantly influenced by vibrational signals of the anions. Moreover, the vibrational features of the selected bands are expected to be influenced by the variety of H-bond interactions with both the anions and the water molecules (Fig. 1). The band at ≈1180 cm^{-1} is related to the C(2)—H and N—H bending modes of the imidazole ring [33]. As discussed above, these are the strong, primary H-donor sites involved in the formation of cation–anion H-bonds and the associated vibrational band is expected to be sensitive to the occurrence of H-bonding modulations among the different ILs. This Raman signal is relatively sharper in the case of [MIM][Cl] with respect to the other ILs (Fig. 2), indicating less structural disorder for the highly symmetric anion. Its frequency position is anion-dependent: ≈1180 cm^{-1} ([Cl]); ≈1180 cm^{-1} ([HSO_4]); ≈1170 cm^{-1} ([NO_3]); ≈1165 cm^{-1} ([TfO]). A red-shift of a bending mode generally indicates a weakening of the related H-bond interactions. Thus, the cation–anion H-bond strength should follow the order: [Cl] ≈[HSO_4] > [NO_3] > [TfO]. This is supported by the T dependence of the band detected for [MIM][HSO_4] in water [33]. It is worth of mention that the trend observed here is in fair agreement with the H-bond basicity scale of the anion based on the solvatochromic β parameter (i.e. [Cl] > [NO_3] > [TfO]) [43]. However, the shape of the anions introduces geometrical factors in the combination of H-bond motives: According to Hunt et al. [43], a different level of complexity should be used in the classification of H-bond for the monoatomic, spherically shaped chloride compared to the more complex, "less symmetric anions with an increasing number of strong H-bond donor sites" [43]. Additionally, a fine tuning of the H-bond acceptor capability of [Cl] and [HSO_4] can be inferred by the band shape of Fig. 2: even if the peak positions are almost coincident, in the case of [HSO_4] the band is asymmetric and skewed to lower wavenumbers, suggesting that, in average, the H-bond acceptor rank should be: [Cl] > [HSO_4]. The band at ≈1450 cm^{-1} is assigned to the deformation of the methyl group, (CH_3), coupled with the stretching of different segments of the imidazole ring. Although the N—CH_3 group is known to show H-bond donor properties stronger than those of the alkyl chain terminal CH_3, as proven in the case of [Cl] counterion in imidazolium based ILs [45], its H-bonding donor capability is expected to be weaker than those of the

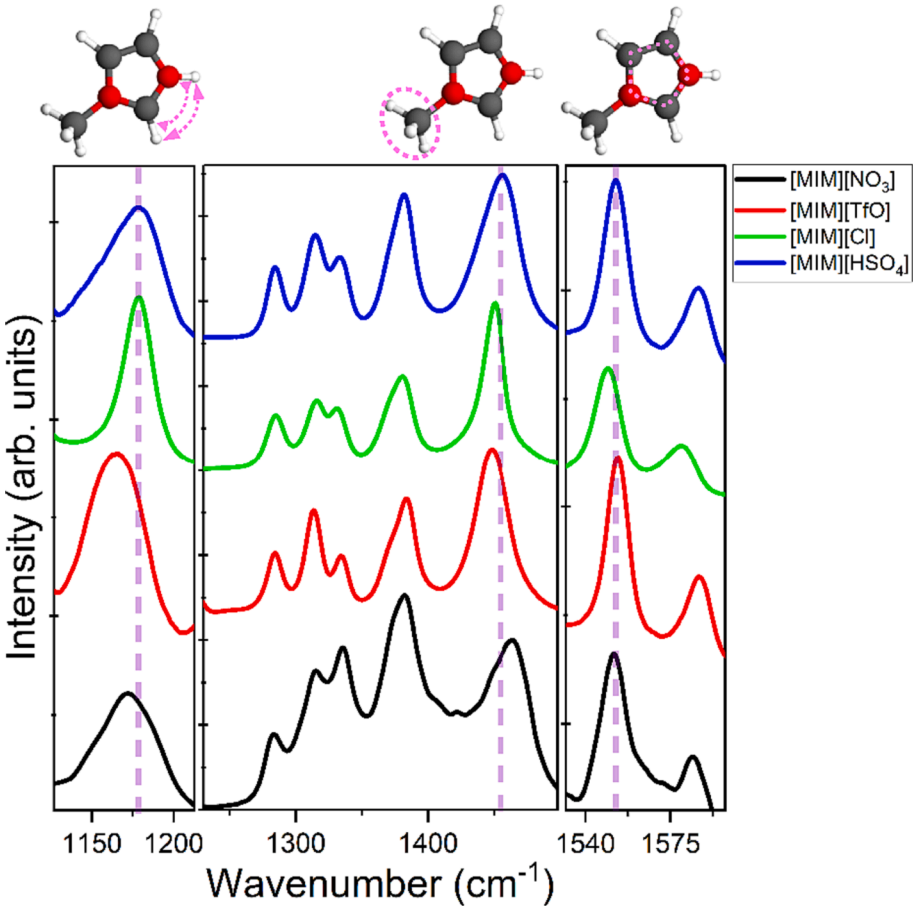

Fig. 2. UVRR (excitation at 266 nm) for the four samples of PILs [MIM][X] in their melted state (spectra collected at temperature of T = 355 K, 368 K, 360 K, and 325 K for [X] = [NO_3], [TfO], [Cl], and [HSO_4], respectively). The sketches at the top show the molecular part of the imidazolium cation mainly involved in the vibrational modes associated to the corresponding Raman peaks marked by the dotted lines, i.e. 1180, 1450 and 1550 cm^{-1}, respectively.

N—H and C(4,5)—H groups. Interestingly, also the position of this band differs for the different systems, suggesting a modulation of the local environment around the group as a function of the anion structure. The band at ≈1550 cm^{-1} is assigned to the asymmetric stretching of the N1—C2—N3 fragment, combined with other segmental motions of the imidazolium ring [30,33,46–48]. Also in this case, small variations in the band position can be observed, indicating changing in the cation environment for the different anions.

The addition of water to PILs leads to significant modifications of the spectral features relative to the Raman signals at ≈ 1180 cm^{-1} and 1450 cm^{-1}, as illustrated in Fig. 3.

In the water-rich domain the first one is found at 1180–1190 cm^{-1} for all the anions, showing in any case similar broadening. In particular, at x_{IL} = 0.005 the band is peaked at ≈1185 cm^{-1} for all the systems, suggesting that in high dilution conditions water molecules tend to replace the anion around the C(2)—H and N—H (hydrophilic moieties), leading to the formation of SSIP and/or SIP species. The observed trends would also suggest that the related cation–anion (double-ionic) H-bonds are weaker than the (ionic) cation-water ones, when [NO_3] and [TfO] are considered, while, in the case of [Cl] and [HSO_4], cation–anion and cation-water H-bonds are of similar extent. This behavior should be mainly ascribed to the H-bonds formed by the N—H group since, as we will discuss later, cation–anion H-bonds formed by the C(2)—H and C(4,5)—H groups are found to be stronger than cation-water ones based on the related stretching modes (see below).

Noticeably also the band at 1450 cm^{-1} is affected by the addition of water and at x_{IL} = 0.005 its position becomes practically the same for all the systems. This suggests that in high diluted conditions, even the more hydrophobic CH_3 moiety of the cation always experiences a similar environment.

A complementary picture of the effect of hydration on the PILs can be achieved by exploring the high frequency range (2800–3800 cm^{-1}) of the UVRR spectra. Here Raman bands arising from the [MIM] species (CH stretching) and water (OH stretching), particularly sensitive to the H-bonding configurations [49–51], can be observed. However, as shown in Fig. 4, considerable overlap between the sharp C—H bands (2800–3300 cm^{-1}) and the broad OH Raman signal of water (2800–3800 cm^{-1}) occurs.

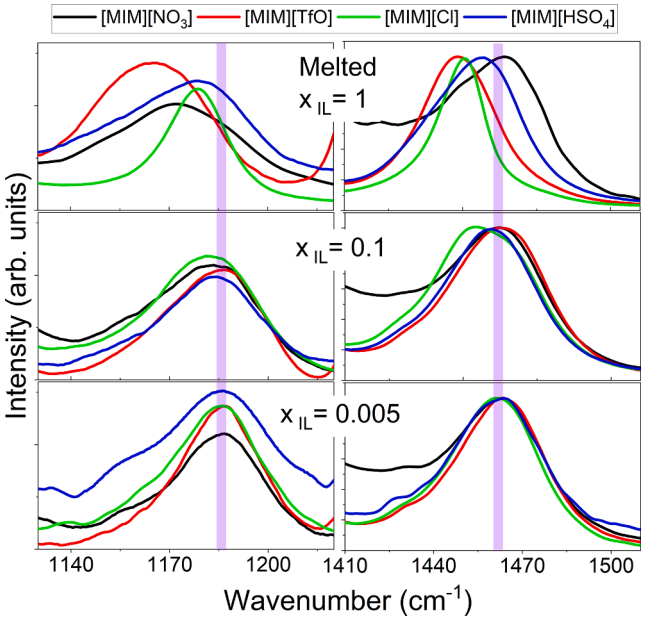

Fig. 3. Comparison among the UVRR spectra of [MIM][X] PILs collected in their melted state and in aqueous solutions (x_{IL} = 0.1 and 0.005) in the two selected wavenumber regions (i.e. at around 1180 and 1460 cm^{-1}, left and right panel respectively). All spectra are normalized to the band around 1460 cm^{-1}.

This spectral region has been analyzed by processing the Raman data with the method proposed by Ben-Amotz et al. [34,35] to extract the so-called solute-correlated (SC) spectra. Along with the disentanglement of the bulk vs. hydration water contribution, the SC spectra also afford a remarkable improvement of the spectral quality for those solute bands overlapped to the contribution of the bulk water in the raw spectrum, as clearly displayed in Fig. 4. Here, the SC spectrum is extracted by using a direct spectral subtraction procedure [35,36], which has proven suitable to get specific information about the hydration water in ILs/water mixtures [39]. In synthesis, the rescaled version of the Raman spectrum of pure water is subtracted from the spectrum of the solution. The rescaling is performed in such a way that the difference spectrum is non-negative and with the minimum area. As an example, Fig. 4 shows the spectrum of diluted [MIM][TfO] in water (x_{IL} = 0.05), the rescaled spectrum of pure water and the resulting SC spectrum. The SC spectrum clearly shows the bands related to CH stretching modes of the methyl group (*ca.* 2850 and 2950 cm^{-1}) and the CH groups of the imidazole ring (*ca.* 3130 and 3190 cm^{-1}) [30,48]. The OH stretching band arising from those water molecules perturbed by the solute (hydrating water) appears in the 3300–3700 cm^{-1} range. The SC-UV Raman spectra obtained for the four samples (x_{IL} = 0.1) are reported in Fig. 5.

To notice that the main features of the CH stretching signals are in general agreement with those of the Raman spectrum of the neat 1-ethylimidazolium nitrate ([EIM][NO_3]) reported by Bernardino and Riberio [52]. The authors nicely demonstrated that in this region the Raman bands can be essentially attributed to the cation CH stretching modes, while the complex spectral distribution observed in the infrared counterpart carries out large contribution from the stretching mode of the NH group, coupled with the cation–anion NH···O H-bond stretching mode. In this respect further progress in the spectral analysis is needed to interpret IR data on PILs looking at this spectral region. Concerning the comparison among the different samples (Fig. 5), the Raman spectra basically show the same components, evidencing some differences in the peak positions, which can be ascribed to the modulations of the H-bond interactions involving the CH groups, especially those of the imidazolium ring.

The wavenumber position of the CH bands, obtained by applying a fitting procedure on the SC spectrum (see Supplementary Material, Fig. S2), is reported in Fig. 6 as a function of x_{IL}. The bands at *ca.* 2830 and 2960 cm^{-1} are attributed to the symmetric and asymmetric CH

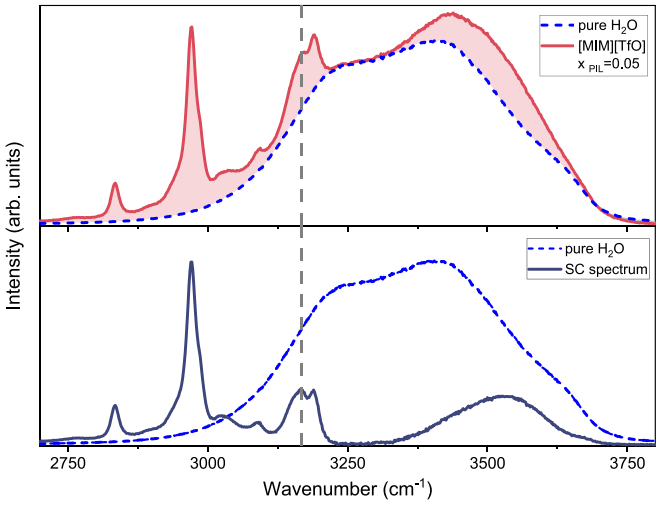

Fig. 4. Upper panel: UVRR spectra of [MIM][TfO]/water solution (x_{IL} = 0.05) together with the rescaled spectrum of neat water (see text for details). The shadow area represents the related solute-correlated (SC) spectrum. Lower panel: the resulting solute-correlated (SC) spectrum compared to the spectrum of pure water. The vertical dotted line indicates the position of the imidazolium C(2)—H stretching mode.

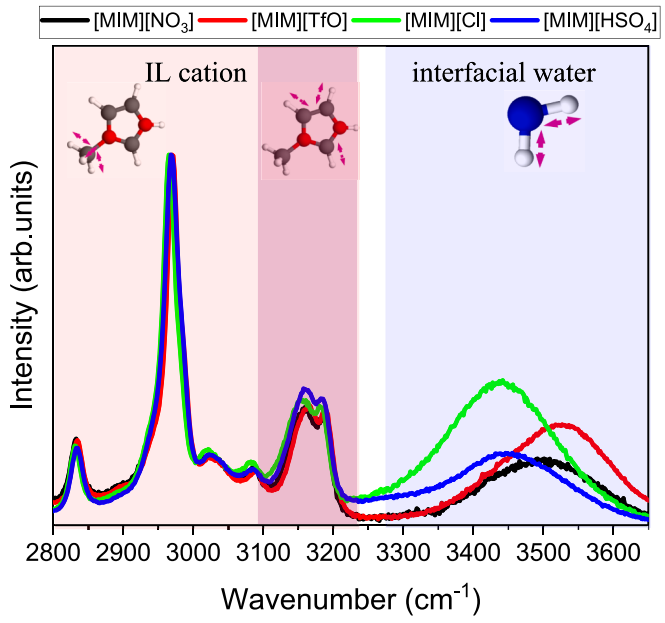

Fig. 5. SC-UV Raman spectra obtained for the [MIM][X] PILs in water (x_{IL} = 0.1)). The spectra have been normalized to the intensity of the CH signals at 2950 cm^{-1}.

stretching modes of the methyl group, respectively. The band at *ca.* 3150 cm^{-1} can be attributed to the C(2)—H stretching mode, while that at *ca.* 3180 cm^{-1} to the C(4,5)—H stretching modes [32,48,53,54]. Also in this case, the position of all these signals converge to the same value for the different samples at the highest dilution, suggesting that in these conditions the cations become evenly hydrated and experience a very similar environment, independently on the anion. This supports the idea at $x_{IL} < 0.05$ SSIP and/or SIP species should prevail. Interestingly, all the bands of [MIM][Cl] show the highest response to concentration changes, with a marked red-shift at increasing x_{IL}. On the other hand, [MIM][TfO] shows more contained changes, while [MIM][NO_3] and [MIM][HSO_4] depict a somewhat intermediate behavior.

The marked, monotonic variation observed for [MIM][Cl] (Fig. 6) points out that the chloride anion acts as an efficient H-bond acceptor toward the cation, effectively replacing the water molecules at increasing PIL concentration. This is very much in line with recent findings [55] on the role of Cl^- in the solvation of choline chloride-based DES and their water mixtures. In the case of the H-bond network of choline chloride-urea/water mixtures, the solvation shell of Cl^- passed progressively from choline-urea interactions to fully hydrated anion with increasing water content, in a continuous competition among the various H-bond donor species. In this competitive coordination of the Cl^- H-bond acceptor, a key role is played also by its size and spherical symmetry. The largest sensitivity shown by the chloride-based PIL, can be then related to the capability of Cl^- to give rise to the variety of H-bond interactions sketched in Fig. 1. The fact that the bands related to C(2)—H and C(4,5)—H bonds red-shift with the increase of x_{IL}, (see Fig. 6c and 6d) also suggests that cation–anion (double-ionic) H-bonds are stronger than cation-water (ionic) H-bonds, as already argued for related AILs [31]. The red shift is particularly relevant for [Cl], while a smaller effect is observed for the less coordinating [TfO].

Information on the molecular state of water hydrating the PILs in the water-rich domain can be derived by the OH stretching distribution (3200–3600 cm^{-1}) in the SC spectra (Fig. 5). These spectra can be mainly attributed to the stretching of hydrating water molecules involved (as H-bond donors) in H-bonds with the anions (H-bond acceptors) [39]. We remark that perturbations on the OH stretch induced by the anion on the (second shell) water-water interactions or induced by the cation are commonly neglected [39,56,57]. The OH stretching bands in the SC spectra are peaked at higher wavenumbers when compared to neat water; this can be related to the anion-induced depletion of the tetrahedral arrangements and vibrational coupling responsible for the component at *ca.* 3200 cm^{-1} prominent in the spectrum of neat water [39,49–51]. The maximum of the OH stretching band observed in the SC spectrum is reported in Fig. 7.

A red-shift of this OH signal implies stronger H-bonding interactions. Thus, the data indicate that water-anion H-bonding strength decreases in the order: [Cl] ~ [HSO_4] > [NO_3] > [TfO], the same deduced before for the (double ionic) cation–anion H-bonds in the neat PILs. The data also indicate that water-anion H-bonding strength shows a certain sensitivity to PIL concentration in the case of [NO_3], [HSO_4], and [Cl], being particularly evident in this latter case for which a global red shift of *ca.* 50 cm^{-1} can be observed. Thus, the data would suggest that water-anion H-bonds are partially modulated by the PIL aggregation, becoming stronger at higher PIL concentrations. A possible explanation

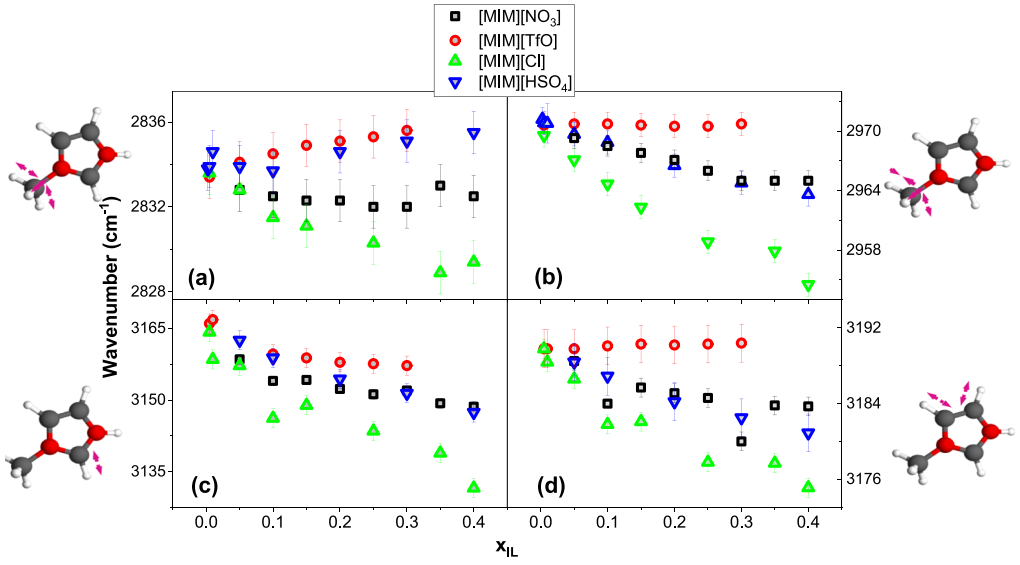

Fig. 6. Wavenumber position of the CH stretching bands in the SC Raman spectra of [MIM][X]/water solutions as a function of concentration, resulting from a fitting procedure (Fig. S2). (a) Symmetric CH stretching of methyl group. (b) Asymmetric CH stretching of methyl group. (c) C(2)—H stretching mode. (d) C(4,5)—H stretching mode.

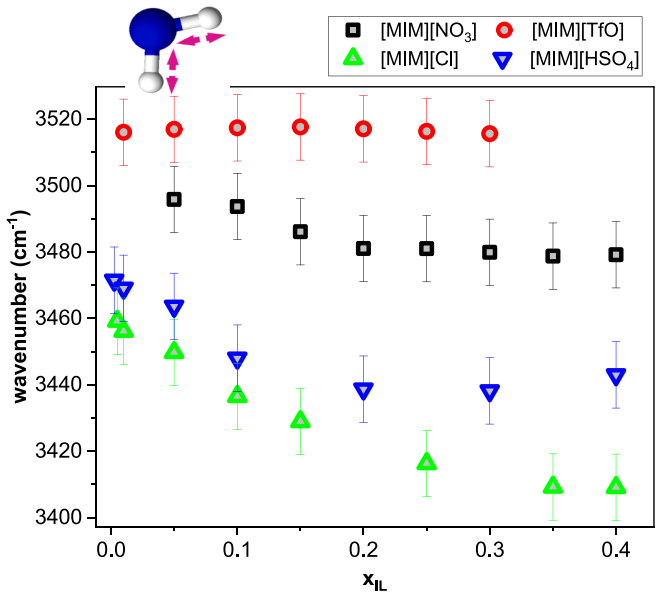

Fig. 7. Maximum of the OH stretching band estimated from the SC spectra of [MIM][X]/water solutions as a function concentration.

could relate to the fact that a fraction of hydrating water molecules might experience multiple interactions with both cations and anions in a polar environment when ionic aggregates (i.e. SSIPs) develop. This effect is not observed in the case of the less coordinating [TfO]. Additional information on the aggregation process can be derived by introducing the hydration number n_h, which represents the (minimum) number of perturbed water molecules per anion [39]. The hydration number n_h can be estimated from the SC spectra according to Eq. (1):

$$n_h = \frac{A_{SC}(OH)}{A_{SOL}(OH)} \times \frac{n_{H_2O}}{n_{IL}} \quad (1)$$

where $A_{SC}(OH)$ and $A_{SOL}(OH)$ are the areas of the OH stretching bands in the SC and the solution spectra (Fig. 4), respectively; n_{H_2O} and n_{IL} the number of molecules of water and PIL in solution, respectively. The n_h values for the four PILs are plotted in Fig. 8 as a function of x_{IL}. For the more diluted solutions $x_{IL} < 0.1$ the resulting n_h values are affected by

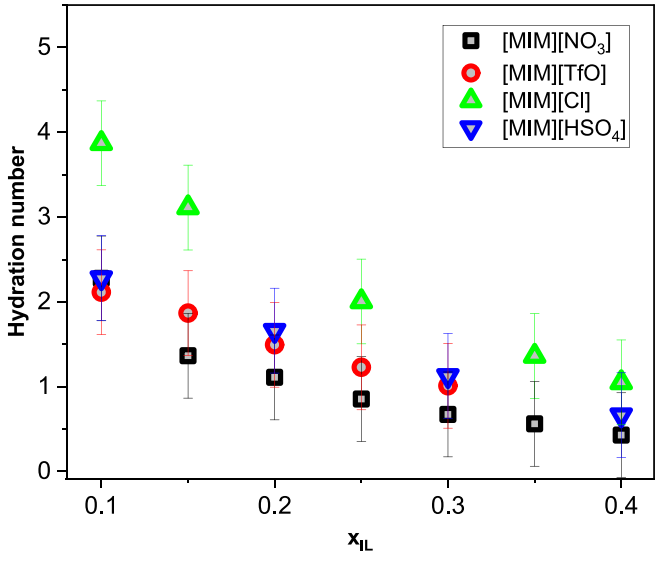

Fig. 8. Hydration number calculated by the Eq. (1) (see details in the text) for the [MIM][X]/water solutions as a function of concentration.

very large uncertainties and are not considered. The n_h of [Cl] is the highest at all x_{IL} values, probably for its high capability of coordination ([Cl] is expected to be *hexa*-coordinated at infinite dilution [55]). On the other hand, the number of affected water molecules is similar for the other anions. With increasing the PIL concentration, n_h decreases for all the samples, evidencing that the formation of CIPs or larger ionic species occurs in the explored concentration range. The effect is particularly evident for the [Cl] in line with its larger aggregation tendency, probably due to its dimension and symmetry.

To note that, based on our estimate, bulk-like water molecules coexist with hydration water molecules in the explored x_{IL} range; in particular, for [MIM][Cl] (other PILs) the percentage of bulk-like water is *ca.* 55 % (*ca.* 75 %) at $x_{IL} = 0.1$ and reduces to *ca.* 35 % (*ca.* 65 %) at $x_{IL} = 0.4$. As a final step, we used the SC Raman spectra to explore the energetics of the water-anion H-bonds based on Eq. (2). This was adapted from the equation applied by Cammarata et al. [56] to calculate, from IR spectra, the H-bonding enthalpy (ΔH^{IR}) in the case of water/IL mixtures, at very low hydration levels. ΔH^{IR} was obtained considering the frequency difference between the asymmetric OH stretching of water in the vapor (ν_3) and in the liquid phases. However, in the Raman spectrum of hydrating water the dominant contribution should come from the symmetric OH stretching modes [39]. Thus, the equation has been modified by introducing the relationship between the asymmetric and symmetric modes of water, proposed by Bricknell et al. [58]. In this way, Eq. (2) is obtained, where ν_3 and ν_1 are the wavenumber of the asymmetric and symmetric stretching of vapor water (ν_3 = 3756 cm^{-1} and ν_1 = 3657 cm^{-1}), respectively, and ν^{IL} is the OH stretching band position in the SC spectrum.

$$\Delta H(kJ/mol) = -335\left[1.17\left(\nu_1 - \nu^{IL}\right) - 0.66\right]/\nu_3 \quad (2)$$

The ΔH values obtained from Eq. (2) considering the data in Fig. 8 ($x_{IL} = 0.05$) are listed in Table 2. There is a reasonable agreement between the calculated values for [MIM][NO_3] and [MIM][TfO] and the ΔH^{IR} values reported in ref. [56]. To note that our estimate refers to hydration water molecules in the water-rich mixtures (when bulk-like water molecules are present and water-water interactions are relevant), while in ref. [56] water confined in very concentrated IL samples was considered.

The ΔH values account for the exothermicity of the interaction between the water and the anion, highlighting the influence of the anion-water interactions in the thermal balance. The data show that ΔH([MIM][Cl]) ~ ΔH([MIM][HSO_4]) ~ ΔH^{IR}(H_2O), thus confirming that [Cl] and [HSO_4] are strong competitor towards water as H-bond acceptor. Conversely, the significantly lower ΔH values obtained for [MIM][NO_3] and [MIM][TfO] further confirm the lower H-bond acceptor capabilities of the nitrate and triflate anions. Basically, our data show that among the studied anions, [Cl] tends to form stronger H-bonds with both the cation and water; thus, to explain its larger aggregation tendency we should also consider its dimensions and symmetry.

To gain some insights of the role of the nature of the cation (protic or aprotic) in shaping hydration properties, a preliminary comparison between the SC Raman spectra of [BMIM][TfO] and [MIM][TfO] has been performed (see Supplementary Material, Fig. S3). The OH stretching band shows similar features in both systems, confirming that the anions

Table 2
Water-anions H-bonding enthalpy ΔH obtained in diluted conditions ($x_{IL} = 0.05$) for the four ILs investigated. ΔH^{IR} are literature values (references in the fifth columns).

Sample	$\nu^{IL}(cm^{-1})$	$-\Delta H\left(\frac{kJ}{mol}\right)$	$-\Delta H^{IR}\left(\frac{kJ}{mol}\right)$	Ref.
[MIM][NO_3]	3500 ± 10	16 ± 1	20.1	[56]
[MIM][TfO]	3520 ± 10	14 ± 1	15.9	[56]
[MIM][Cl]	3450 ± 10	22 ± 1		
[MIM][HSO_4]	3460 ± 10	20 ± 1		
H_2O			23.0	[4]

play a major role in determining the water H-bonding properties. Nevertheless, a relative blue-shift of the band is detected for [MIM][TfO], indicating slightly weaker water-anion interactions. At the same time the average hydration number at around $x_{IL} = 0.1$ is larger for [BMIM][TfO] ($n_h \sim 3.8 \pm 0.5$ [39]) than [MIM][TfO] ($n_h = 2.2 \pm 0.5$). Thus, the data evidence that the cation partially affects both aggregation and water hydration properties. In particular, the formation of ionic aggregates seems favored in the [MIM][TfO] (PIL) when compared to [BMIM][TfO] (AIL). This might be related to the possibility of the smaller protic cation to form additional cation–anion (double-ionic) H-bond with the available N–H group.

4. Conclusions

In this work, we used UV Raman spectroscopy to obtain deep insights on the strength and distribution of the intermolecular H-bonding in aqueous solutions of a set of model methylimidazolium-based PILs in the water-rich regime, when ionic aggregates and bulk-like water domains do coexist. A direct spectral subtraction procedure has been employed in the CH and OH stretching region to determine the solute-correlated (SC) spectra, emphasizing the spectral modifications induced by the solute on the surrounding water (hydration water). The combined analysis of the SC-UV Raman spectra and of several diagnostic Raman bands of the [MIM] cation, allowed us to extract information on the H-bonding features and aggregation of [MIM][X] solutions for different anions ([X] = [Cl], [HSO_4], [NO_3], [TfO]). The analysis of the neat PILs suggested that the proton-acceptor capability changes in the order [Cl] ~ [HSO_4] > [NO_3] > [TfO] for the (double-ionic) cation–anion H-bonds, in line with the reported H-bond basicity values [40,42]. The addition of water to PILs modulates the cation environment and at high dilution ($x_{IL} < 0.05$) similar hydration features emerge, independently of the type of anion. This suggests that in the diluted regime solvent-shared ion pairs (SSIP) and/or solvent-separated ion pairs (SIP) would prevail over contact ion pairs (CIP) and/or larger ionic aggregates. Interestingly, our data would suggest that for the [NO_3]- and [TfO]-based PILs, cation-water (ionic) H-bonds formed by the NH group are stronger than the double-ionic cation–anion ones, indicating that water might tend to preferentially hydrate this group.

Spectral variations clearly indicate the formation of cation–anion H-bonds through the cation C(2)—H and C(4,5)—H ring groups at increasing x_{IL} (starting from $x_{IL} \sim 0.05$), especially evident in the case of [MIM][Cl]. These (double-ionic) H-bonds are stronger than the (ionic) cation-water ones. Likely, the proton-acceptor capability, size and symmetry of Cl^- facilitate the formation of multiple interactions around the cation and the creation of an extended H-bond network among the ionic species. The aggregation tendency decreases for the [NO_3] and [HSO_4] anions, and further reduces in the case of the weakest H-bond acceptor [TfO]. Anyhow, also in this latter case, the formation of cation–anion H-bonds with the C(2)—H is still detectable, suggesting the formation of isolated contact ion pairs (CIP).

Specific information on the hydration water around the anions were obtained by analyzing the SC-UV Raman spectra in the OH stretching region. Also in this case the strength of water-anion H-bonding is found to depend on the anion basicity: [Cl] ~ [HSO_4] > [NO_3] > [TfO]. This strength is independent on concentration in the case of [MIM][TfO], while it increases with x_{IL} in the case of [NO_3], [HSO_4] and [Cl], following the basicity trend. This strengthening of water-anion interactions is particularly relevant for [MIM][Cl]. The calculated hydration number n_h indicates that [Cl] perturbs a higher number of water molecules than the other anions. Moreover, the larger n_h decrease with x_{IL} observed for [MIM][Cl] supports its greater tendency to progressively form contact ion pairs (CIPs) and larger ionic aggregates. At the same time, hydration water molecules experience a reinforcement of H-bonding interactions, probably due to their involvement in multiple interactions with both anion and cation (i.e. SSIPs), within a polar environment. The energetics of the H-bonds involved in the hydration process in the water-rich domain can be also worked out from Raman data. We reported a significant decrease in the hydration enthalpies going from [Cl] (22 kJ/mol) and [HSO_4] (20 kJ/mol) to [NO_3] (16 kJ/mol) and [TfO] (14 kJ/mol). Thus, the larger propensity of [Cl] to form ionic aggregates should be ascribed to the synergy of different factors such as the reduced size (higher charge density), spherical symmetry, and high H-bond basicity. Finally, a preliminary comparison between spectral features observed for the PIL [MIM][TfO] and the AIL [BMIM][TfO] indicates that changing the nature of the cation might partially modulate both water H-bonding and aggregation. More specifically, the formation of ionic aggregates seems favored for [MIM][TfO], likely due to its protic nature. Further studies will be performed comparing other PIL and AIL to clarify the situation and to understand to what extent the observed trends can be generalized.

CRediT authorship contribution statement

F. Matroodi: Formal analysis, Investigation, Methodology, Validation, Writing – original draft. **C. Bottari:** Formal analysis, Investigation, Methodology. **B. Rossi:** Conceptualization, Data curation, Resources, Validation, Writing – review & editing. **A. Mannu:** Formal analysis, Investigation, Methodology. **M. Paolantoni:** Conceptualization, Formal analysis, Methodology, Writing – original draft, Writing – review & editing. **A. Mele:** Conceptualization, Investigation, Methodology, Writing – original draft, Writing – review & editing.

Declaration of competing interest

The authors declare that they have no known competing financial interests or personal relationships that could have appeared to influence the work reported in this paper.

Data availability

Data will be made available on request.

Acknowledgments

FM gratefully acknowledges funding by TRIL Program of the Abdus Salam International Centre for Theoretical Physics (ICTP). MP acknowledges funding by the European Union–NextGeneration EU under the Italian Ministry of University and Research (MUR) National Innovation Ecosystem grant ECS00000041–Vitality. AM would like to thank Politecnico di Milano for granting a one-year sabbatical at Elettra Sincrotrone. Part of the research was carried out within the MICS (Made in Italy – Circular and Sustainable) Extended Partnership and received funding from the European Union Next-Generation EU (PIANO NAZIONALE DI RIPRESA E RESILIENZA (PNRR) – MISSIONE 4 COMPONENTE 2, INVESTIMENTO 1.3 – D.D. 1551.11-10-2022, PE00000004). This manuscript reflects only the authors' views and opinions, neither the European Union nor the European Commission can be considered responsible for them.

Appendix A. Supplementary material

Supplementary data to this article can be found online at https://doi.org/10.1016/j.molliq.2023.123881.

References

[1] J.P. Hallett, T. Welton, Room-temperature ionic liquids: Solvents for synthesis and catalysis. 2, Chem. Rev. 111 (2011).
[2] T.L. Greaves, C.J. Drummond, Protic ionic liquids: properties and applications, Chem. Rev. 108 (2008) 206–237.
[3] T.L. Greaves, C.J. Drummond, Protic ionic liquids: evolving structure–property relationships and expanding applications, Chem. Rev. 115 (2015) 11379–11448.

[4] K. Dong, S. Zhang, Hydrogen bonds: a structural insight into ionic liquids, Chem. Eur. J. 18 (2012) 2748–2761.
[5] K. Fumino, A. Wulf, R. Ludwig, The potential role of hydrogen bonding in aprotic and protic ionic liquids, PCCP 11 (2009) 8790–8794.
[6] K. Fumino, A. Wulf, R. Ludwig, Strong, localized, and directional hydrogen bonds fluidize ionic liquids, Angew. Chemie Int. Ed. 47 (2008) 8731–8734.
[7] K. Fumino, A. Wulf, R. Ludwig, Hydrogen bonding in protic ionic liquids: reminiscent of water, Angew. Chemie Int. Ed. 48 (2009) 3184–3186.
[8] C. Ma, A. Laaksonen, C. Liu, X. Lu, X. Ji, The peculiar effect of water on ionic liquids and deep eutectic solvents, Chem. Soc. Rev. 47 (2018) 8685–8720.
[9] M. Chen, G. Feng, R. Qiao, Water-in-salt electrolytes: An interfacial perspective, Curr. Opin. Colloid Interface Sci. 47 (2020) 99–110.
[10] A. Sanati, M.R. Malayeri, O. Busse, J.J. Weigand, Utilization of ionic liquids and deep eutectic solvents in oil operations: progress and challenges, J. Mol. Liq. (2022) 119641.
[11] J. Hehe, N. Guanhua, Z. Chuanjie, Z. Xiangfei, S. Gongshuai, W. Zhenyang, H. Qiming, Molecular dynamics simulations and experimental characterization of the effect of different concentrations of [Bmim][Cl] in aqueous solutions on the wettability of anthracite, Fuel 324 (2022) 124618.
[12] J. Chen, W. Zhou, Y. Quan, B. Liu, M. Yang, M. Chen, X. Han, X. Xu, P. Zhang, S. Shi, Ionic liquid additive enabling anti-freezing aqueous electrolyte and dendrite-free Zn metal electrode with organic/inorganic hybrid solid electrolyte interphase layer, Energy Storage Mater. 53 (2022) 629–637.
[13] C.A. Summers, R.A. Flowers, Protein renaturation by the liquid organic salt ethylammonium nitrate, Protein Sci. 9 (2000) 2001–2008.
[14] A. Kumar, P. Venkatesu, Overview of the stability of α-chymotrypsin in different solvent media, Chem. Rev. 112 (2012) 4283–4307.
[15] G. Rai, A. Kumar, Elucidation of ionic interactions in the protic ionic liquid solutions by isothermal titration calorimetry, J. Phys. Chem. B 118 (2014) 4160–4168.
[16] K.S. Egorova, A.V. Posvyatenko, S.S. Larin, V.P. Ananikov, Ionic liquids: prospects for nucleic acid handling and delivery, Nucleic Acids Res. 49 (2021) 1201–1234.
[17] Y. Shao, G. Yin, Z. Wang, Y. Gao, Proton exchange membrane fuel cell from low temperature to high temperature: material challenges, J. Power Sources 167 (2007) 235–242.
[18] L. Zhang, J. Zhang, D.P. Wilkinson, H. Wang, Progress in preparation of non-noble electrocatalysts for PEM fuel cell reactions, J. Power Sources 156 (2006) 171–182.
[19] B. Wang, Recent development of non-platinum catalysts for oxygen reduction reaction, J. Power Sources 152 (2005) 1–15.
[20] M. Anouti, J. Jacquemin, D. Lemordant, Transport properties of protic ionic liquids, pure and in aqueous solutions: Effects of the anion and cation structure, Fluid Phase Equilib. 297 (2010) 13–22.
[21] G. Rai, A. Kumar, Interesting thermal variations owing to cationic ring structural features in protic ionic liquids, PCCP 15 (2013) 8050–8053.
[22] E. Bodo, S. Mangialardo, F. Capitani, L. Gontrani, F. Leonelli, P. Postorino, Interaction of a long alkyl chain protic ionic liquid and water, J. Chem. Phys. 140 (2014) 204503.
[23] T.-M. Chang, L.X. Dang, R. Devanathan, M. Dupuis, Structure and dynamics of N, N-Diethyl-N-methylammonium triflate ionic liquid, neat and with water, from molecular dynamics simulations, Chem. A Eur. J. 114 (2010) 12764–12774.
[24] W. Li, Z. Zhang, B. Han, S. Hu, Y. Xie, G. Yang, Effect of water and organic solvents on the ionic dissociation of ionic liquids, J. Phys. Chem. B 111 (2007) 6452–6456.
[25] P. Stange, K. Fumino, R. Ludwig, Ion speciation of protic ionic liquids in water: transition from contact to solvent-separated ion pairs, Angew. Chemie Int. Ed. 10 (2013) 2990–2994.
[26] B. Golub, K. Fumino, P. Stange, V. Fossog, R. Hempelmann, D. Ondo, D. Paschek, R. Ludwig, Balance between contact and solvent-separated ion pairs in mixtures of the protic ionic liquid [Et3NH][MeSO3] with water controlled by water content and temperature, J. Phys. Chem. B 125 (2021) 4476–4488.
[27] I. Vázquez-Fernández, A. Bouzina, M. Raghibi, L. Timperman, J. Bigarré, M. Anouti, Influence of hydrophilic/hydrophobic protic ionic liquids (PILs) on the poly (vinylidene fluoride)(PVDF-ionic liquid) membrane properties, J. Mater. Sci. 55 (2020) 16697–16717.
[28] Z. Liu, S.Z. El Abedin, F. Endres, Raman and FTIR spectroscopic studies of 1-ethyl-3-methylimidazolium trifluoromethylsulfonate, its mixtures with water and the solvation of zinc ions, ChemPhysChem 16 (2015) 970–977.
[29] H.E. Bailey, Y.-L. Wang, M.D. Fayer, Impact of hydrogen bonding on the dynamics and structure of protic ionic liquid/water binary mixtures, J. Phys. Chem. B 121 (2017) 8564–8576.
[30] V.H. Paschoal, L.F.O. Faria, M.C.C. Ribeiro, Vibrational spectroscopy of ionic liquids, Chem. Rev. 117 (2017) 7053–7112.
[31] D.K. Pandey, P. Sanchora, D. Rana, P. Donfack, A. Materny, D.K. Singh, Impact of water on the hydrogen bonding between halide-based ion-pairs investigated by Raman scattering and density functional theory calculations, J. Raman Spectrosc. 51 (2020) 147–164.
[32] B.A. Marekha, M. Bria, M. Moreau, I. De Waele, F.-A. Miannay, Y. Smortsova, T. Takamuku, O.N. Kalugin, M. Kiselev, A. Idrissi, Intermolecular interactions in mixtures of 1-n-butyl-3-methylimidazolium acetate and water: Insights from IR, Raman, NMR spectroscopy and quantum chemistry calculations, J. Mol. Liq. 210 (2015) 227–237.
[33] C. Bottari, B. Rossi, A. Mele, A. Damin, S. Bordiga, M. Musso, A. Gessini, C. Masciovecchio, Synchrotron-based UV resonance Raman scattering for investigating ionic liquid-water solutions, Condens. Matter Phys. 22 (2019) 43301.
[34] P. Perera, M. Wyche, Y. Loethen, D. Ben-Amotz, Solute-induced perturbations of solvent-shell molecules observed using multivariate Raman curve resolution, J. Am. Chem. Soc. 130 (2008) 4576–4577.
[35] D. Ben-Amotz, Hydration-shell vibrational spectroscopy, J. Am. Chem. Soc. 141 (2019) 10569–10580.
[36] K.R. Fega, A.S. Wilcox, D. Ben-Amotz, Application of Raman multivariate curve resolution to solvation-shell spectroscopy, Appl. Spectrosc. 66 (2012) 282–288.
[37] J.G. Davis, K.P. Gierszal, P. Wang, D. Ben-Amotz, Water structural transformation at molecular hydrophobic interfaces, Nature 491 (2012) 582–585.
[38] D.S. Wilcox, B.M. Rankin, D. Ben-Amotz, Distinguishing aggregation from random mixing in aqueous t-butyl alcohol solutions, Faraday Discuss. 167 (2013) 177–190, https://doi.org/10.1039/c3fd00086a.
[39] C. Bottari, L. Almásy, B. Rossi, B. Bracco, M. Paolantoni, A. Mele, Interfacial water and microheterogeneity in aqueous solutions of ionic liquids, J. Phys. Chem. B (2022).
[40] H. Niedermeyer, C. Ashworth, A. Brandt, T. Welton, P.A. Hunt, A step towards the a priori design of ionic liquids, PCCP 15 (2013) 11566–11578.
[41] S. Zhang, X. Qi, X. Ma, L. Lu, Y. Deng, Hydroxyl ionic liquids: the differentiating effect of hydroxyl on polarity due to ionic hydrogen bonds between hydroxyl and anions, J. Phys. Chem. B 114 (2010) 3912–3920.
[42] L.E. Shmukler, I.V. Fedorova, Y.A. Fadeeva, L.P. Safonova, The physicochemical properties and structure of alkylammonium protic ionic liquids of RnH4-nNX (n= 1–3) family. A mini–review, J. Mol. Liq. 321 (2021) 114350.
[43] P.A. Hunt, C.R. Ashworth, R.P. Matthews, Hydrogen bonding in ionic liquids, Chem. Soc. Rev. 44 (2015) 1257–1288.
[44] F. D'amico, M. Saito, F. Bencivenga, M. Marsi, A. Gessini, G. Camisasca, E. Principi, R. Cucini, S. Di Fonzo, A. Battistoni, UV resonant Raman scattering facility at Elettra, Nucl. Instruments Methods Phys. Res. Sect. A Accel. Spectrometers, Detect. Assoc. Equip. 703 (2013) 33–37.
[45] J.D. Holbrey, W.M. Reichert, M. Nieuwenhuyzen, S. Johnson, K.R. Seddon, R. D. Rogers, Crystal polymorphism in 1-butyl-3-methylimidazolium halides: supporting ionic liquid formation by inhibition of crystallization, Chem. Commun. (2003) 1636–1637.
[46] D.A. Carter, J.E. Pemberton, Raman spectroscopy and vibrational assignments of 1- and 2-methylimidazole, J. Raman Spectrosc. 28 (1997) 939–946.
[47] R.W. Berg, J.N. Canongia Lopes, R. Ferreira, L.P.N. Rebelo, K.R. Seddon, A. A. Tomaszowska, Raman spectroscopic study of the vapor phase of 1-methylimidazolium ethanoate, a protic ionic liquid, Chem. A Eur. J. 114 (2010) 10834–10841.
[48] S.A. Katsyuba, P.J. Dyson, E.E. Vandyukova, A.V. Chernova, A. Vidiš, Molecular structure, vibrational spectra, and hydrogen bonding of the ionic liquid 1-ethyl-3-methyl-1H-imidazolium tetrafluoroborate, Helv. Chim. Acta 87 (2004) 2556–2565.
[49] M.E. Gallina, P. Sassi, M. Paolantoni, A. Morresi, R.S. Cataliotti, Vibrational analysis of molecular interactions in aqueous glucose solutions. Temperature and concentration effects, J. Phys. Chem. B 110 (2006) 8856–8864.
[50] M. Paolantoni, N.F. Lago, M. Albertí, A. Laganà, Tetrahedral ordering in water: Raman profiles and their temperature dependence, Chem. A Eur. J. 113 (2009) 15100–15105.
[51] C. Bottari, L. Comez, M. Paolantoni, S. Corezzi, F. D'Amico, A. Gessini, C. Masciovecchio, B. Rossi, Hydration properties and water structure in aqueous solutions of native and modified cyclodextrins by UV R aman and Brillouin scattering, J. Raman Spectrosc. 49 (2018) 1076–1085.
[52] K. Bernardino, M.C.C. Ribeiro, Hydrogen-bonding and symmetry breaking in the protic ionic liquid 1-ethylimidazolium nitrate, Vib. Spectrosc 120 (2022) 103358.
[53] A. Wulf, K. Fumino, R. Ludwig, Comment on "New Interpretation of the CH Stretching Vibrations in Imidazolium-Based Ionic Liquids", Chem. A Eur. J. 114 (2010) 685–686, https://doi.org/10.1021/jp9080146.
[54] T. Masaki, K. Nishikawa, H. Shirota, Microscopic study of ionic liquid– H2O systems: alkyl-group dependence of 1-alkyl-3-methylimidazolium cation, J. Phys. Chem. B 114 (2010) 6323–6331.
[55] M.E. Di Pietro, O. Hammond, A. van den Bruinhorst, A. Mannu, A. Pádua, A. Mele, M.C. Gomes, Connecting chloride solvation with hydration in deep eutectic systems, PCCP 23 (2021) 107–111.
[56] L. Cammarata, S.G. Kazarian, P.A. Salter, T. Welton, Molecular states of water in room temperature ionic liquids, PCCP 3 (2001) 5192–5200.
[57] P.N. Perera, B. Browder, D. Ben-Amotz, Perturbations of water by alkali halide ions measured using multivariate Raman curve resolution, J. Phys. Chem. B (2009) 1805–1809.
[58] B.C. Bricknell, T.A. Ford, T.M. Letcher, Spectroscopic and thermodynamic properties of hydrogen bonded water molecules in binary liquid mixtures, Spectrochim. Acta Part A: Mol. Biomol. Spectrosc. 53 (1997) 299–315.